



**HAL**  
open science

## Influence of sliding interfaces on the response of a viscoelastic pavement

Olivier Chupin, Armelle Chabot

► **To cite this version:**

Olivier Chupin, Armelle Chabot. Influence of sliding interfaces on the response of a viscoelastic pavement. 6th Int. Conf. on Maintenance and Rehabilitation of Pavements and Technological control, MAIREPAV6 (Print ISBN 978-88-8202-0293), Jul 2009, Politecnico Di Torino, Italy. pp.675. hal-00402109

**HAL Id: hal-00402109**

**<https://hal.science/hal-00402109>**

Submitted on 16 Jul 2023

**HAL** is a multi-disciplinary open access archive for the deposit and dissemination of scientific research documents, whether they are published or not. The documents may come from teaching and research institutions in France or abroad, or from public or private research centers.

L'archive ouverte pluridisciplinaire **HAL**, est destinée au dépôt et à la diffusion de documents scientifiques de niveau recherche, publiés ou non, émanant des établissements d'enseignement et de recherche français ou étrangers, des laboratoires publics ou privés.

# Influence of sliding interfaces on the response of a viscoelastic pavement

O. Chupin & A. Chabot

Laboratoire Central des Ponts et Chaussées, Bouguenais Cedex, France

**ABSTRACT:** This article aims at analyzing the influence of the perfect-slip interface condition on the computed response of a pavement structure. This condition has been implemented in the ViscoRoute software that solves the 3D mechanical problem of a multilayered viscoelastic pavement under moving loads. In the calculations, the load speed is assumed to be constant and the viscoelastic behavior of asphalt layers is represented by the Huet-Sayegh model. The dynamic equations are first solved in the frequency domain. A Fast Fourier Transformation is then employed to get the solution in the spatial domain. The effect of sliding interfaces and temperature are analyzed through an example dealing with composite pavements. In this context, the designing fields commonly used in France appear to be strongly influenced by the viscoelastic behavior of asphalt layers and the interlayer condition. This influence is quite noticeable on the deflection.

## 1 INTRODUCTION

Since early works by Sneddon (1952), the theoretical response of a half-space under a moving load with static and dynamic components has been largely investigated. Among all the applications covered by this field one can refer to seismic problems, road and high speed railways engineering. In the pavement framework, three-dimensional Finite Element-based models have been proposed (e.g. Heck et al. 1998, Elseifi et al. 2006). However, these models may be hard to manipulate and to offer fast alternative tools, semi-analytical methods are still developed (Hopman 1996, Siddharthan et al. 1998). In France, at LCPC, Duhamel et al. (2005) developed such a model which is implemented in the ViscoRoute software. This program directly integrates the viscoelastic behavior of asphalt materials through the Huet-Sayegh model which is particularly well-suited for the modeling of asphalt overlays (Huet 1999, Sayegh 1965). The ViscoRoute kernel has been validated by comparison to analytical solutions (semi-infinite medium), Finite Element simulations (multilayered structure), and results obtained for multiple loads in the context of the A380 pavement experimental program (Chabot et al. 2006). It has been shown that for bituminous wearing courses and thick flexible pavement structures, especially for aircraft structure and low traffic, other design concepts than usual ones need to be developed. Until now, all these developments have been done by considering perfectly bonded interfaces between layers of the structure. Nevertheless, due to the significant influence of the bonding quality at an interface on the pavement life at long term, different types of interlayer conditions must be investigated. This remark is especially true for composite pavements as those studied by Chea et al. (2008) and Chabot et al. (2008).

In this framework, the present article is outlined as follows: the implementation of the sliding interlayer condition in ViscoRoute is first explained. Then, the effect of the sliding interlayer condition on the mechanical response of a composite pavement is analyzed. This analysis is conducted upon deflection, strains and normal stresses computed at different depths within the

structure. The influence of temperature is also studied since it affects the viscoelastic behavior of asphalt layers.

## 2 RESPONSE OF A VISCOELASTIC PAVEMENT TO A MOVING LOAD

This section briefly describes the modeling of the perfectly slip interface condition and its implementation in the ViscoRoute kernel.

### 2.1 Governing equations

The pavement structure is assimilated to a semi-infinite multilayered medium composed of  $n$  horizontal layers that have either an elastic or a viscoelastic behavior. The structure is solicited by one or several loads moving at constant speed in the  $x$ -direction, and applied at the free surface of the medium. Inertial forces are considered in the problem modeling which is governed by the elastodynamic equations. These equations are solved for each layer in a moving basis attached to the load. One shifts from the fixed basis  $(x, y, z)$ , tied to the medium, to the moving basis  $(X, Y, Z)$  by making the following change of variable:

$$x = X + Vt; \quad y = Y; \quad z = Z \quad (1)$$

The elastodynamic equations, with no body forces, expressed in the moving basis  $(X, Y, Z)$  reads for layer  $i$ :

$$\text{Div}(\boldsymbol{\sigma}(X, Y, Z)) = \rho_i V^2 \frac{\partial^2 \mathbf{u}(X, Y, Z)}{\partial X^2} \quad (2)$$

$\rho_i$  denotes the density of the  $i$ th layer. Boundary and interlayer conditions are required to solve Equation 2. These are detailed in section 2.2.

### 2.2 Solution in the frequency domain and interlayer conditions

Analytical solutions to Equation 2 are computed in the frequency domain in which the viscoelastic constitutive law takes the same form as Hooke's law. It reads:

$$\boldsymbol{\sigma}^*(k_1, k_2, Z) = 2\mu_i^*(k_1 V) \boldsymbol{\varepsilon}^*(k_1, k_2, Z) + \lambda_i^*(k_1 V) \text{tr}(\boldsymbol{\varepsilon}^*(k_1, k_2, Z)) \mathbf{I} \quad (3)$$

The complex Lamé coefficients,  $\lambda_i^*(k_1 V)$  and  $\mu_i^*(k_1 V)$ , depend on the complex modulus  $E_i^*(k_1 V)$  of the  $i$ th layer in the same way as in the elastic case. A Fourier transform applied in the  $X$  and  $Y$  directions to Equation 2 combined with Equation 3 yields:

$$\mathbf{A}_i \frac{\partial^2 \mathbf{u}^*(k_1, k_2, Z)}{\partial Z^2} + \mathbf{j} \mathbf{B}_i \frac{\partial \mathbf{u}^*(k_1, k_2, Z)}{\partial Z} - \mathbf{C}_i \mathbf{u}^*(k_1, k_2, Z) = \mathbf{0} \quad (4)$$

where  $k_1$  and  $k_2$  are the wave numbers and  $j$  is the imaginary unit.  $\mathbf{u}^*$  is the displacement field expressed in the frequency domain. Matrices  $\mathbf{A}_i$ ,  $\mathbf{B}_i$  and  $\mathbf{C}_i$  are given by Equation 5:

$$\mathbf{A}_i = \begin{pmatrix} c_{si}^2 & 0 & 0 \\ 0 & c_{si}^2 & 0 \\ 0 & 0 & c_{pi}^2 \end{pmatrix}, \quad \mathbf{B}_i = \begin{pmatrix} 0 & 0 & k_1(c_{pi}^2 - c_{si}^2) \\ 0 & 0 & k_2(c_{pi}^2 - c_{si}^2) \\ k_1(c_{pi}^2 - c_{si}^2) & k_2(c_{pi}^2 - c_{si}^2) & 0 \end{pmatrix} \quad (5)$$

$$\mathbf{C}_i = \begin{pmatrix} k_1^2(c_{pi}^2 - V^2) + k_2^2 c_{si}^2 & k_1 k_2(c_{pi}^2 - c_{si}^2) & 0 \\ k_1 k_2(c_{pi}^2 - c_{si}^2) & k_1^2(c_{si}^2 - V^2) + k_2^2 c_{pi}^2 & 0 \\ 0 & 0 & k_1^2(c_{si}^2 - V^2) + k_2^2 c_{si}^2 \end{pmatrix}$$

where  $c_{si}$  and  $c_{pi}$  denote the dilatation and the shear wave velocities of layer  $i$ , respectively. These matrices gather the material properties of layer  $i$ . After some mathematical manipulation, the solution to Equation 4 is obtained and reads:

$$\begin{aligned}
\mathbf{u}_1^*(k_1, k_2, Z) &= k_1 \beta_{1i}^- e^{-\kappa_{pi} Z} + \kappa_{si} \beta_{3i}^- e^{-\kappa_{si} Z} + k_1 \beta_{1i}^+ e^{\kappa_{pi} Z} - \kappa_{si} \beta_{3i}^+ e^{\kappa_{si} Z} \\
\mathbf{u}_2^*(k_1, k_2, Z) &= k_2 \beta_{2i}^- e^{-\kappa_{pi} Z} + \kappa_{si} \beta_{2i}^- e^{-\kappa_{si} Z} + k_2 \beta_{2i}^+ e^{\kappa_{pi} Z} - \kappa_{si} \beta_{2i}^+ e^{\kappa_{si} Z} \\
\mathbf{u}_3^*(k_1, k_2, Z) &= j \kappa_{pi} \beta_{1i}^- e^{-\kappa_{pi} Z} + j k_2 \beta_{2i}^- e^{-\kappa_{si} Z} + j k_1 \beta_{3i}^- e^{-\kappa_{si} Z} \\
&\quad - j \kappa_{pi} \beta_{1i}^+ e^{\kappa_{pi} Z} + j k_2 \beta_{2i}^+ e^{\kappa_{si} Z} + j k_1 \beta_{3i}^+ e^{\kappa_{si} Z}
\end{aligned} \tag{6}$$

In Equation 6,  $\kappa_{pi}$  and  $\kappa_{si}$  are the longitudinal and the shear wave numbers of layer  $i$ . Besides, the stress tensor is obtained from the displacement field and the constitutive law. The displacement field depends on 6 parameters that are representative of a layer. The solution is completely defined once these parameters have been calculated. They are determined from the boundary and the interlayer conditions that yield the 6n equations required to set all the parameters. Boundary conditions on the free surface (imposed force vector on the loading area) and at infinity (radiation condition) result in 6 equations. The remaining equations are provided by the interlayer relations.

In the case of a bonded interface, the continuity relation (Equation 7) is used. This relation stipulates that the displacements and the traction vector from both sides of an interface are equal at the  $Z$ -coordinate of this interface. The continuity equation for an interface squeezed between layers  $i$  and  $i+1$  reads:

$$\begin{bmatrix} \mathbf{u}^*(k_1, k_2, Z) \\ \boldsymbol{\sigma}^*(k_1, k_2, Z) \cdot \mathbf{e}_Z \end{bmatrix}_i = \begin{bmatrix} \mathbf{u}^*(k_1, k_2, Z) \\ \boldsymbol{\sigma}^*(k_1, k_2, Z) \cdot \mathbf{e}_Z \end{bmatrix}_{i+1} \tag{7}$$

On the other hand, the sliding interlayer condition states that the shear components of the traction vector are equal to zero at both side of an interface. In the same time, the conditions on the vertical displacement and the third component of the traction vector remain the same as in Equation 7. The sliding interlayer condition for an interface settled between layer  $i$  and  $i+1$  reads:

$$\begin{pmatrix} \mathbf{u}_3^*(k_1, k_2, Z) \\ \sigma_{13}^*(k_1, k_2, Z) \\ \sigma_{23}^*(k_1, k_2, Z) \\ 0 \\ 0 \\ \sigma_{33}^*(k_1, k_2, Z) \end{pmatrix}_i = \begin{pmatrix} \mathbf{u}_3^*(k_1, k_2, Z) \\ 0 \\ 0 \\ \sigma_{13}^*(k_1, k_2, Z) \\ \sigma_{23}^*(k_1, k_2, Z) \\ \sigma_{33}^*(k_1, k_2, Z) \end{pmatrix}_{i+1} \tag{8}$$

Globally, the interlayer condition (bonded or sliding case) can be expressed as a function of the amplitude vectors  $\boldsymbol{\beta}_i$  and  $\boldsymbol{\beta}_{i+1}$  whose components are the  $\beta$ -parameters of Equation 6:

$$(\mathbf{M}_i) \cdot \boldsymbol{\beta}_i = (\mathbf{N}_{i+1}) \cdot \boldsymbol{\beta}_{i+1} \tag{9}$$

where,

$$\boldsymbol{\beta}_i = \{ \beta_{1i}^-, \beta_{2i}^-, \beta_{3i}^-, \beta_{1i}^+, \beta_{2i}^+, \beta_{3i}^+ \} \tag{10}$$

The 6-by-6 matrices  $\mathbf{M}_i$  and  $\mathbf{N}_{i+1}$  integrate the constitutive behavior of layers  $i$  and  $i+1$  and depend on the displacement or the stress components invoked by the interlayer relation.  $\mathbf{M}_i$  and  $\mathbf{N}_{i+1}$  are the same for the continuity equation but not for the sliding interlayer relation. These matrices are not detailed herein. They are derived from Equations 6, 7, 8, and the traction vector ensued from the displacement field.

To compute all the amplitude vectors, the boundary and the interlayer conditions are assembled in a global matrix. A linear system of unknown the amplitude vector (Equation 11) is then solved.

$$\begin{bmatrix} \mathbf{D}_0 & & & & & \\ \mathbf{M}_1 & -\mathbf{N}_2 & & & & \mathbf{0} \\ & \ddots & & & & \\ & & \mathbf{M}_i & -\mathbf{N}_{i+1} & & \\ \mathbf{0} & & & \ddots & & \\ & & & & \mathbf{M}_{n-1} & \mathbf{D}_n \end{bmatrix} \begin{Bmatrix} \vdots \\ \vdots \\ \vdots \\ \beta_i \\ \beta_{i+1} \\ \vdots \\ \vdots \end{Bmatrix} = \begin{Bmatrix} \mathbf{f} \\ \mathbf{0} \\ \vdots \\ \vdots \\ \mathbf{0} \end{Bmatrix} \quad (11)$$

$\mathbf{D}_0$  and  $\mathbf{D}_n$  reflect the boundary conditions on the free surface and at infinity, respectively.  $\mathbf{f}$  denotes the imposed force vector expressed in the frequency domain. Equation 11 is solved by using a pivoting method.

We implemented the method developed in this section in the ViscoRoute kernel (Duhamel et al. 2005) which uses the C++ language programming. The implementation of the sliding interface condition has been validated in elasticity by comparison with software ALIZE-LCPC that computes the Burmister solution of the elastic problem.

### 2.3 Solution in the spatial domain

Once a solution in displacement or stress is computed in the frequency domain, The Fast Fourier Transform (FFT) is utilized to evaluate the integral that leads to the response in the spatial domain. The FFT is run in two dimensions for all values of  $k_1$  and  $k_2$  but  $k_1$  equal zero. In the latter case, the integrand is singular, though still integrable, and a different method based on Gauss-Legendre polynomials is used. For more details, see Duhamel et al. (2005).

## 3 APPLICATION TO A COMPOSITE PAVEMENT

In this section, the afore-developed method is used to analyze the mechanical response of a composite pavement under a single dual-wheel load. The effect of sliding interfaces and temperature is analyzed.

### 3.1 Material, structure and loading characteristics

A composite pavement composed of four layers is studied. The different layers are defined as follows: a surface course of bituminous materials (BBSG), a base layer of bituminous materials (GB), a layer of materials treated with hydraulic binders (GC), and a pavement foundation. BBSG, GB and GC stand for semi-coarse bituminous concrete, base asphalt concrete and cement bound graded aggregates, respectively.

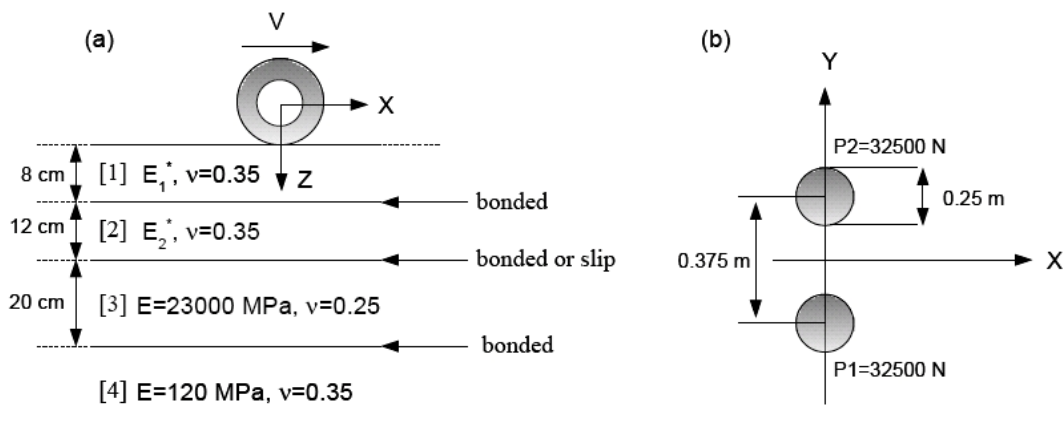


Figure 1. Sketch of the composite pavement and the loading conditions.

As shown in Figure 1, a slip interface condition can be introduced between layers 2 and 3, i.e. between the asphalt and the concrete cement layers.

Layers of a composite pavement are initially bonded. However, due to repeated loading and differential expansion between the base of layer 2 and layer 3, the bonding between the asphalt concrete and the material treated with hydraulic binders may eventually fail (Setra-LCPC 1997). Consequently, the effects of the sliding interface condition on the mechanical response of the pavement structure is investigated by introducing sliding between these two layers.

The loading is defined by a classical single dual-wheel configuration represented by two loads exerting a uniformly distributed pressure of 0.622 MPa onto two disks of radius 0.125 m, with a center-to-center distance of 0.375 m (see Fig. 1).

Asphalt layers are modeled according to the Huet-Sayegh model (Huet 1963, Sayegh 1965) while other layers follow Hooke's law. In the frequency domain, the complex modulus of the Huet-Sayegh model depends on the load speed and the temperature. It is given by Equation 12:

$$E^*(k_1 V, \theta) = E_0 + \frac{E_\infty - E_0}{1 + \delta \left( i k_1 V \tau(\theta) \right)^{-k} + \left( i k_1 V \tau(\theta) \right)^{-h}} \quad (12)$$

$E_0$  is the static elastic modulus,  $E_\infty$  is the instantaneous elastic modulus,  $k$  and  $h$  are exponents of the parabolic dampers ( $1 > h > k > 0$ ), and  $\delta$  is a positive non-dimensional coefficient balancing the contribution of the first damper in the global behavior.  $\theta$  denotes the temperature and  $\tau$  is a response time parameter governed by Equation 13:

$$\tau(\theta) = \exp\left(A_0 + A_1 \theta + A_2 \theta^2\right) \quad (13)$$

where  $A_0$ ,  $A_1$  and  $A_2$  are constant parameters. A schematic representation of the Huet-Sayegh rheological model is given in Figure 2. Parameters of this model are determined based on experimental data stemming from complex modulus tests performed at different temperatures and frequencies, and by using software Viscoanalyse (Chailleux et al. 2006). The parameter values corresponding to the materials involved in this study are summarized in Table 1.

Table 1. Parameters of the Huet-Sayegh model for layers 1 and 2.

	Einf Mpa	E0 MPa	$\delta$	k	h	A0	A1	A2
[1] : BBSG	40995	18	2.356	0.186	0.515	2.2387	-0.3996	0.00152
[2] : GB	38814	31	1.872	0.178	0.497	2.5320	-0.3994	0.00175

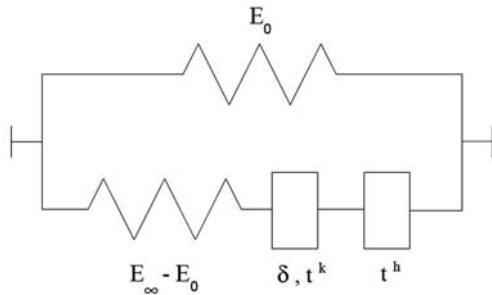


Figure 2. Schematic representation of the Huet-Sayegh model.

### 3.2 Effects of sliding interfaces on the computed fields

In this section, the mechanical response of the structure is computed for two types of the inter-layer condition between layers 2 (BB) and 3 (GC): either a full bonded or a perfectly slip interface is considered at this location. The other interfaces within the structure are assumed to be bonded.

Mechanical fields computed for the bonded condition are compared to those obtained for the sliding interlayer condition. The vertical displacement (or deflection,  $u_z$ ) on the free surface of the pavement, the longitudinal/transversal strains in the X and Y directions ( $\epsilon_{xx}$ ,  $\epsilon_{yy}$ ), at the base

of the asphalt layers ( $Z=0.199$  m), the vertical strain ( $\epsilon_{zz}$ ) in soil, and the normal stresses ( $\sigma_{xx}$ ,  $\sigma_{yy}$ ) at the base of the concrete layer ( $Z=0.399$  m) are investigated. In this analysis, the load velocity and the temperature are set to 20 m/s and 15°C, respectively.

Figure 3 is dedicated to the vertical displacement on the free surface of the structure. Figure 3a shows the comparison between the longitudinal section (in  $Y=0$ ) of the vertical displacement computed in the sliding (triangular markers) and the bonded (circular markers) cases. See Figure 1 for the definition of the  $X$  and the  $Y$  axis. Figure 3b displays similar quantities but in the  $Y$ -direction (in  $X=0$ ). The curves plotted in Figure 3a and 3b show that the maximum of the deflection is twice larger for a slip interface between layers 2 and 3. The order of magnitude of the deflection is quite the same in the  $X$  and  $Y$  directions. Based on these observations, the deflection could be proposed as an indicator to evaluate layer-debonding of a pavement.

Figure 4 shows the longitudinal strains at the base of the concrete layer. Positive values relate to extension and negative values to contraction. On the left (Fig. 4a),  $\epsilon_{xx}$  is plotted against  $X$  (in  $Y=0$ ) because the maximum value of this strain component is situated on the  $X$ -axis. In the bonded case (circular markers), the deformation along the  $X$ -axis is in contraction and the curve is asymmetric due to viscoelastic effects. When a slip interface is introduced between layers 2 and 3, extension appears and, as expected, the maximum of  $\epsilon_{xx}$  is largely greater than in the bonded case. Similar trends are observed for  $\epsilon_{yy}$  which is plotted versus  $Y$  (in  $X=0$ ) in Figure 4b.

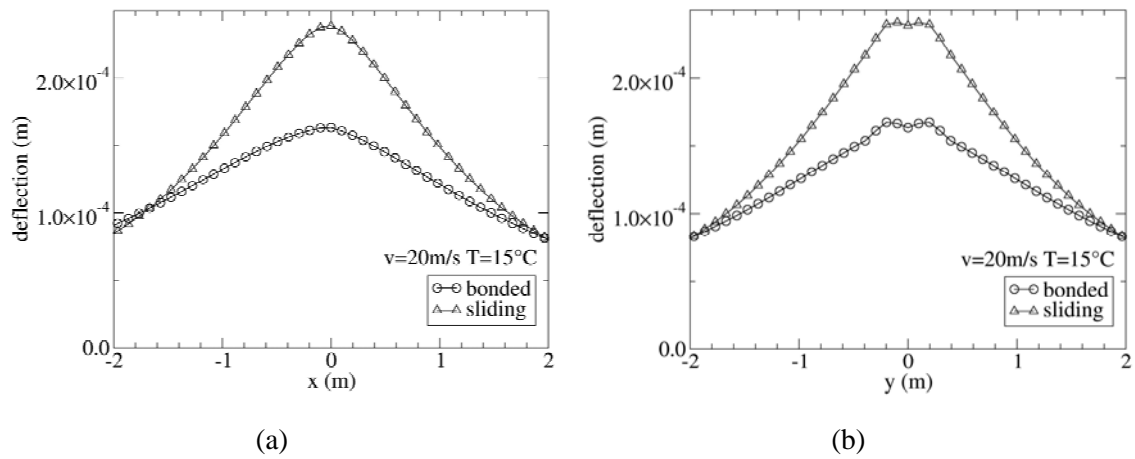


Figure 3. (a) Comparison of the deflection obtained for the bonded and the sliding condition: longitudinal section in the  $X$  direction ( $Y=0$ ). (b) The same as (a) but in the  $Y$  direction ( $X=0$ ).

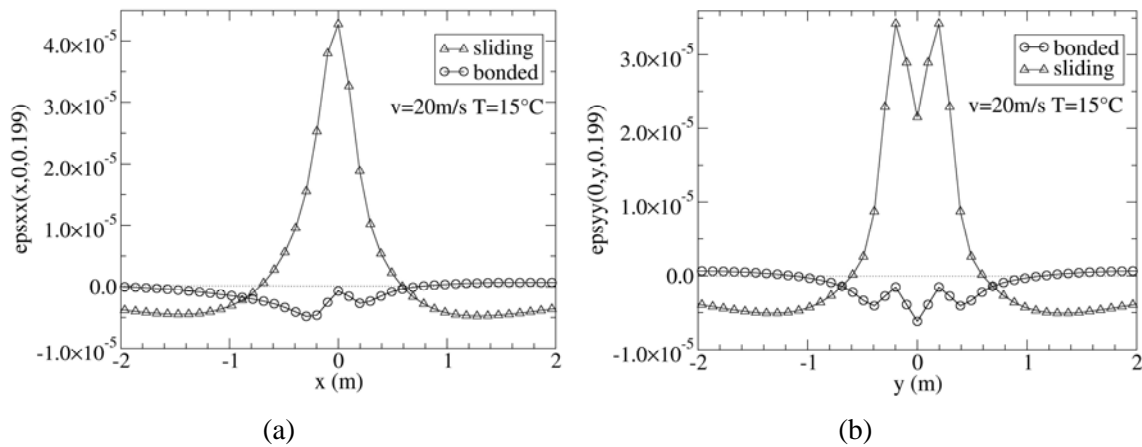


Figure 4. (a) Longitudinal section (in  $Y=0$  and  $Z=0.199$  m) of  $\epsilon_{xx}$  computed in the sliding and the bonded cases. (b) The same as (a) but for  $\epsilon_{yy}$  plotted in the  $Y$  direction ( $X=0$ ).

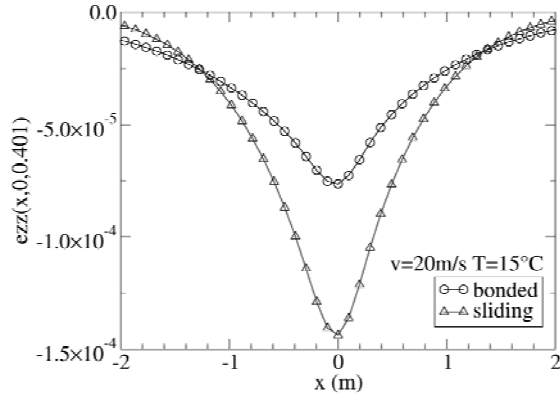


Figure 5. Comparison between  $\varepsilon_{zz}$  computed with the sliding and the bonded interface condition: longitudinal section in the X direction ( $Y=0$ ).

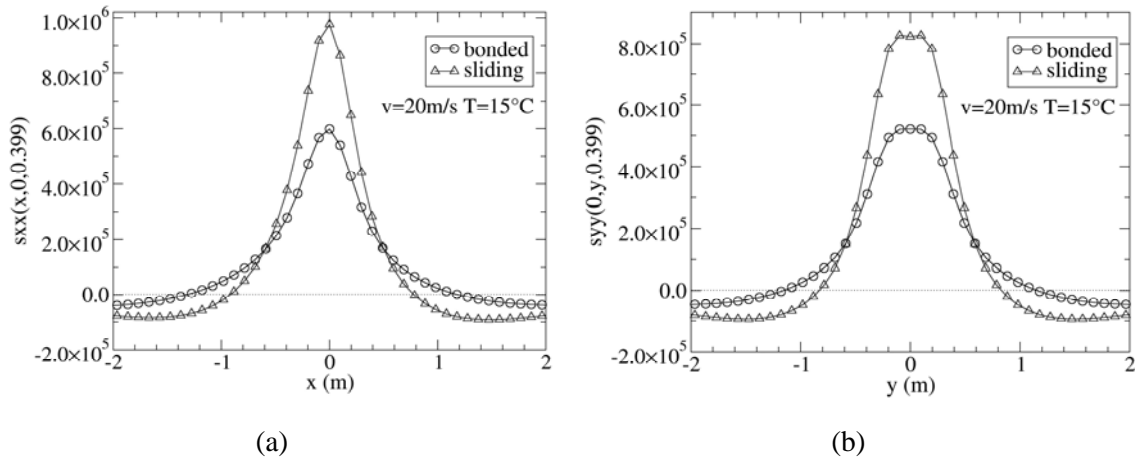


Figure 6. (a) Longitudinal section (in  $Y=0$  and  $Z=0.399$  m) of  $\sigma_{xx}$  computed in the sliding and the bonded cases. (b) The same as (a) but for  $\sigma_{yy}$  plotted in the Y direction ( $X=0$ ).

Similar qualitative results, i.e. higher deformation for the perfect-slip condition, are observed for  $\varepsilon_{zz}$  which is plotted in Figure 5. In the present example, switching from a bonded to a sliding interface condition results in vertical strains in soil that are multiplied by two at maximum.

Figure 6 is devoted to the normal stress at the base ( $Z=0.399$  m) of the concrete layer. Positive values of the normal stress characterize a tensile stress whereas negative values relate to a compressive stress. Figure 6a displays  $\sigma_{xx}$  along a longitudinal section (in  $Y=0$ ) for both bonded (circular markers) and sliding (triangular markers) cases. The shape of the curves is similar for the two types of interface although the slip interface leads to higher values of  $\sigma_{xx}$ . Tensile stresses are much larger than compressive stresses that develop away from the imposed loads. Similar remarks also apply to  $\sigma_{yy}$  which is plotted along the Y-axis (in  $X=0$ ) in Figure 6b. Note that the maximum of  $\sigma_{yy}$  is located on this axis.

### 3.3 Influence of temperature

Asphalt layers have a thermo-viscoelastic behavior modeled by the Huet-Sayegh model. The mechanical response of the whole structure is thus dependent of the temperature within these layers. To quantify the influence of temperature on the pavement response, the deflection is computed for two different temperatures:  $15^\circ\text{C}$  and  $35^\circ\text{C}$ . The higher the temperature the more viscous get the asphalt layers. In this section, the load velocity is kept equal to 20 m/s.

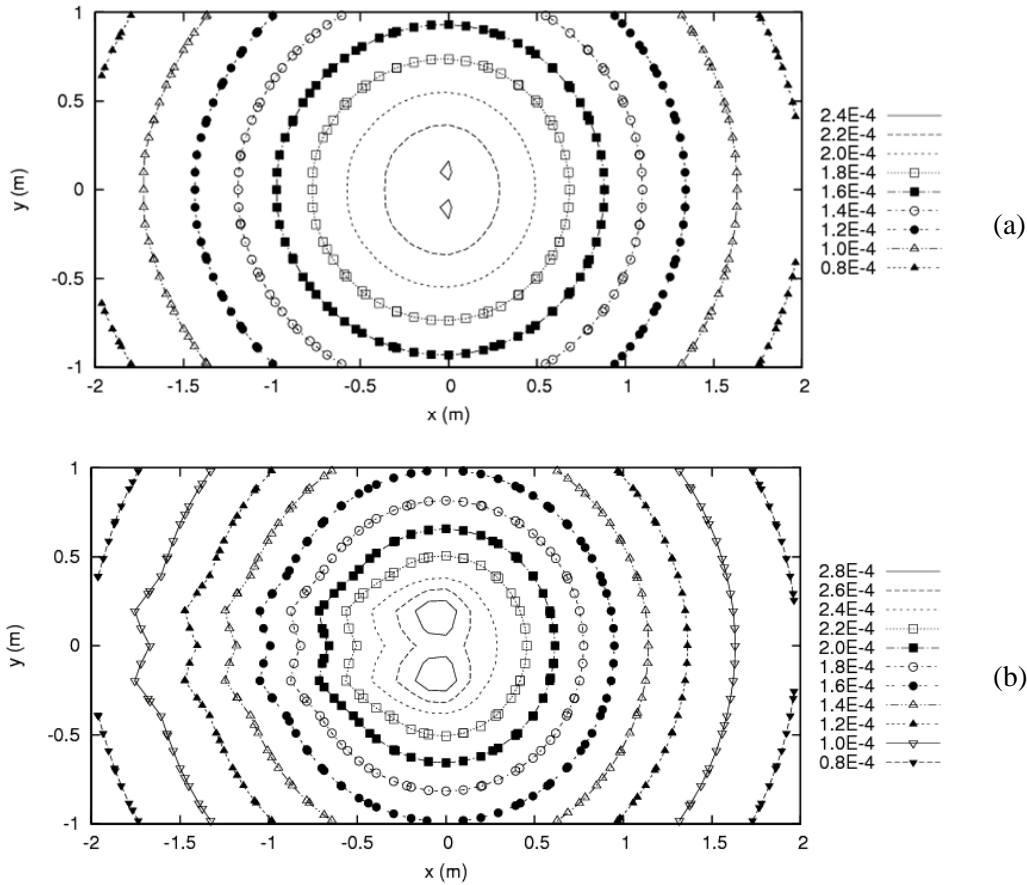


Figure 7. Isovalues of the deflection at 15°C (a) and 35°C (b) obtained in the case of sliding interfaces.

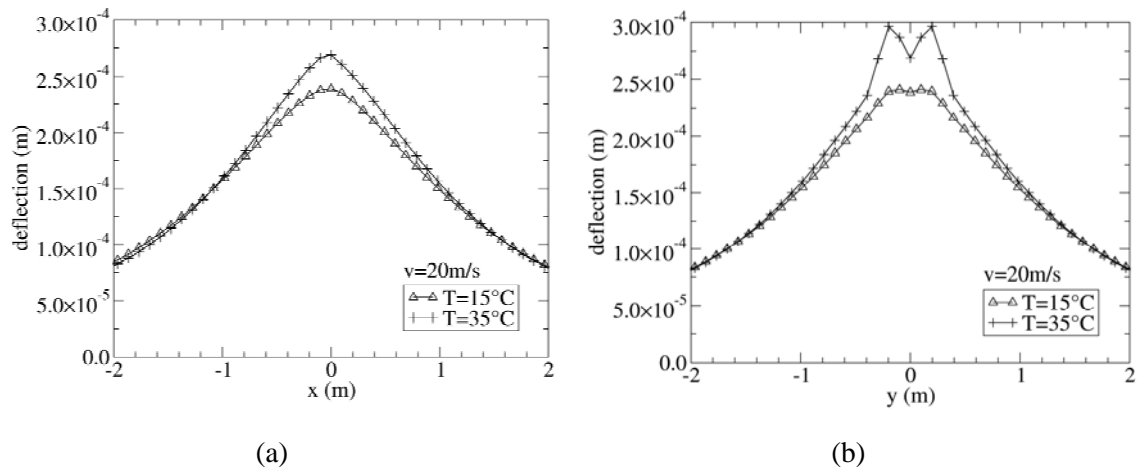


Figure 8. (a) Comparison of the deflection computed for a temperature of 15°C and 35°C (sliding case): longitudinal section in the X-direction (Y=0). (b) The same as (a) but plotted along the Y-direction (X=0).

Figure 7 displays isovalues of the deflection computed for the slip interface between layers 2 and 3. At the top (Fig. 7a), isovalues of the deflection obtained at T=15°C are plotted in the X-Y plan. Most of these isovalues have a circular shape and exhibit a quite symmetrical response of the vertical displacement (close to an elastic response). The highest values of the deflection are

obviously located next to the applied load. At this location, the shape of the isovalues are different and let us perceive the presence of the two separate loads applied on the pavement. The maximum value of the vertical displacement is about 0.24 mm. On the other hand, Figure 7b shows isovalues of the deflection at a temperature equal to 35°C. As expected, the magnitude of the deflection is higher for a temperature of 35°C. Moreover, the isovalues are not circular at this temperature. The two wheels leave some sort of a trail at the rear of the loading indicating that the deflection is significantly affected by the viscoelastic behavior of the pavement.

The order of magnitude of the deflection is the same in both directions at a temperature of 15°C. However, the deflection is higher in the Y direction than in the X direction as the temperature increases. The prints left by the separate wheels are also more pronounced at a temperature of 35°C, especially in the Y direction (Fig. 8b). To complete these observations, the effect of a non uniform loading have to be analyzed.

#### 4 CONCLUSION

The perfect-slip condition has been successfully implemented in the ViscoRoute program that solves the mechanical problem of a multilayered viscoelastic pavement under moving loads. Multilayered structures with bonded and/or sliding interfaces can now be treated by the extended version of this program. Quantitative results on the influence of the slip interlayer condition have been presented in terms of deflection and designing fields commonly used in France. These results have been obtained for a particular composite pavement. As expected, the introduction of a slip interface within a multilayered pavement led to higher values of the aforementioned fields. Due to the thermo-viscoelastic behavior of asphalt layers, these fields also increased with temperature. These effects are quite noticeable on the deflection.

Modeling the response of pavement structures that incorporate slip interfaces could help the development of methods for the detection of interface flaws. The analysis presented herein should be deepened to achieve this goal. If needed in forthcoming developments, a friction law at interfaces could also be easily implemented.

#### REFERENCES

- Chabot, A., Tamagny, P., Duhamel, D. & Poché, D., 2006. Visco-elastic modeling for asphalt pavements – software ViscoRoute. *10th International Conference on Asphalt Pavements*, 12-17 August, Québec, Canada.
- Chabot, A., Pouteau, B., Balay, J.-M., De Larrard, F., 2008. FABAC Accelerated Loading Test of Bond between Cement Overlay and Asphalt layers. *Sixth International RILEM Conference Cracking in Pavements*, June 16-18, Chicago, US. In Taylor & Francis Group Proceedings, ISBN 13: 978-0-415-47575-4, 13-23.
- Chailleux, E., Ramond, G., Such, C. & de la Roche, C. 2006. A mathematical-based master-curve construction method applied to complex modulus of bituminous materials. *Roads Materials and Pavement Design*, 7 (EATA Special Issue): 75-92.
- Chea, S., Martinez, J. 2008. Using surface deflection for detection of interface damage between pavement layers. *Roads Materials and Pavement Design* (special issue EATA 2008): 359-372.
- Duhamel, D., Chabot, A., Tamagny, P. & Harfouche, L. 2005. Viscoroute: Visco-elastic modeling for asphalt pavements - Viscoroute : Modélisation des chaussées bitumineuses. *Bulletin des Laboratoires des Ponts et chaussées* (<http://www.lcpc.fr/en/sources/blpc/index.php>). (258-259): 89-103.
- Elseifi, M.A., Al-Qadi, I.L. & Yoo, P.J. 2006. Viscoelastic Modeling and Field Validation of Flexible Pavements. *Journal of Engineering Mechanics (ASCE)*, 132 (2): 172-178.
- Heck, J.V., Piau, J.M., Gramsammer, J.C., Kerzreho, J.P. & Odeon, H. 1998. Thermo-visco-elastic modelling of pavements behaviour and comparison with experimental data from LCPC test track. *Proc. of the 5<sup>th</sup> BCRA, Trondheim, Norway 6-8 July 1998*.
- Hopman, P.C. 1996. VEROAD: A Viscoelastic Multilayer Computer Program. *Transportation Research Record*. 1539: 72-80.
- Huet, C. 1963. *Etude par une méthode d'impédance du comportement viscoélastique des matériaux hydrocarbonés*. Ph.D. dissertation, Université de Paris.
- Huet C. (1999). Coupled size and boundary-condition effects in viscoelastic heterogeneous and composite bodies. *Mechanics of Materials*. (31): 787-829.

- Siddharthan, R.V., Yao, J., & Sebaaly, P.E. 1998. Pavement strain from moving dynamic 3D load distribution. *Journal of Transportation Engineering*. 124(6): 557-566.
- Sayegh, G. (1965). Contribution à l'étude des propriétés viscoélastiques des bitumes purs et des bétons bitumineux, *Ph.D. dissertation*, Faculté des Sciences de Paris.
- Setra-LCPC 1997. *French Design Manual For Pavement Structures*. Laboratoire Central des Ponts et Chaussées and Service d'Etudes Techniques des Routes et Autoroutes, 247 pages.
- Sneddon, I.N. 1952. The stress produced by a pulse of pressure moving along the surface of a semi-infinite solid. *Rend. Circ. Mat. Palermo*. 2: 57-62.